Supporting Information

Bozec et al. - Trade-offs between fisheries harvest and the resilience of coral reefs

SI Methods

I. Demographic model of parrotfish populations

Model structure. Caribbean populations of parrotfish were modeled using a length-structured matrix model that accounts for size-dependent growth, mortality and settlement. For a vector $\mathbf{n}_t$ of fish density in every length class at the start of time step t, the density-at-length vector after one time increment is given by the difference equation:

$$\mathbf{n}_{t+1} = [\ \mathbf{G}\ (\mathbf{n}_t + \mathbf{r})\ ] \circ \mathbf{s} \qquad \textbf{[S1]}$$

where **G** is a length-specific growth transition matrix, **r** is a density-at-length vector of fish recruits, and **s** is a vector of survivorship (the open dot represents element-wise multiplication). With this order of multiplication, fish recruit first, then grow, then survive.

Length-specific growth transition matrices describe the proportion of individuals growing from one length class to another for a given unit of time (1–3). Transition proportions are described by a probability distribution with mean and variance representing the average and individual variability in growth increments for a given size class. Here, the growth transition matrix was built using the R package *fishmethods* (4) following the method of Chen et al. (5), where growth increments are determined by the von Bertalanffy growth function (VBGF), and where individuals are normally distributed around each average length increment with a non-constant variance across size classes. Generating the matrix of size transitions in this way requires the specification of the size-class scheme (each class being represented by its midpoint value), and the VBGF parameters L_∞ (asymptotic length) and K (Brody's growth coefficient) as well as empirical estimates of their respective standard errors and correlation to allow the estimation of variability in growth increments. In the resulting matrix, fish either stay at their original length or move to a larger size class. The largest size class acts as a plus group with a probability of 1 of remaining in the class.

The vector of recruitment **r** represents the number of fish that settle onto the reef at the beginning of a time step. Here settlers were assigned to the first size class (1 cm fork length, FL) based on empirical evidence that parrotfish settle at 8−10 mm standard length (6, 7). Recruitment was assumed to be independent of adult population size, due to high larval connectivity among reefs and the prevalence of post-settlement compensatory mechanisms [e.g., density-dependent mortality (8)].

The vector of survivorship **s** gives the proportion of fish in each length class that escape mortality during a time step:

$$\mathbf{s} = \exp (- \mathbf{z}) \quad \textbf{[S2]}$$

where **z** is a vector of total instantaneous mortality at length defined by:

$$\mathbf{z} = \mathbf{m}_{\mathbf{pred}} + \mathbf{m}_{\mathbf{sen}} + F\,\mathbf{p} \quad \textbf{[S3]}$$

The vectors $\mathbf{m}_{\mathbf{pred}}$ and $\mathbf{m}_{\mathbf{sen}}$ give the length-specific instantaneous rates of mortality due to predation and senescence, respectively. F (scalar) is the instantaneous rate of fishing mortality, and **p** a vector of probability of capture (fishing gear selectivity) at length. Empirical evidence suggests that parrotfish (9–11) and coral reef fish in general (12, 13) experience disproportionate mortalities at settlement and increasing survival as fish grow. Mortality due to predation was thus assumed to decrease at an exponential rate with parrotfish size:

$$\mathbf{m}_{\mathbf{pred}} = \alpha_{pred} \exp (\beta_{pred}\,\mathbf{l}), \text{ with } \beta_{pred} < 0 \quad \textbf{[S4]}$$

where **l** is a vector of body lengths (FL) associated to the density-at-length vector.

Oppositely, mortality due to senescence was assumed to increase exponentially with size, with the implicit assumption that size and age are correlated. Here, the probability of death was adjusted to the range of body lengths exhibited by the modeled species:

$$\mathbf{m}_{\mathbf{sen}} = \alpha_{sen} \exp (\beta_{sen}\,\mathbf{l} / L_{\infty}), \text{ with } \beta_{sen} > 0 \quad \textbf{[S5]}$$

With constant rates of settlement, growth and survival in each size class, population abundance as modeled by Eq. S1 will asymptotically reach, from any initial condition (i.e., any initial vector of density-at-length), a deterministic equilibrium with a stable size distribution (2). Early attempts at computing the growth transition matrix showed that three months was the optimal time step to adequately describe the process of growth. With a shorter time step, the predicted length increment for large fish was less than 1 cm, meaning that these fish were unable to grow. Longer time steps produced length increments that were too great for small fish, so that many juvenile classes would not be represented by the model.

Model parametrization and calibration. Parametrization of the model of parrotfish populations was performed using a long-term survey of the stoplight parrotfish, *Sparisoma viride* (Bonnaterre, 1788), conducted on the leeward coast of Bonaire Island, Netherlands Antilles ["Karpata" site (14)]. Early surveys (Aug. 1988−Sep. 1989) showed an increase in population abundance and average body length, possibly responding to a macroalgal rise triggered by the mass mortality of

the urchin *Diadema antilarum* (15). However, surveys from December 1989 to January 1992 (24 months) indicated a fairly constant abundance and population size structure. In the absence of parrotfish fishing at the time of the survey (16–18), the stoplight parrotfish dataset was assumed to be representative of an unfished population (i.e., $F = 0$ for all lengths).

Maximum length was chosen to coincide with L_∞ which was assumed to be 39 cm FL based on the maximum length reported during the 1988−92 visual surveys and catch-and-release data from the same site [475 caught fish with no individuals greater than 40 cm FL (19)]. Brody's growth coefficient K was empirically estimated based on a log-log relationship between K and L_∞ values (7, 20) established using data for eight parrotfish species from the Caribbean (Fig. S1*A*) based on mark-recapture (21) and age determination studies (7, 17, 22):

$$\text{Log } K = -0.90 \text{ Log } L_\infty + 2.80 \qquad \textbf{[S6]}$$

A value of 0.61 yr^{-1} for K was subsequently adopted for the corresponding $L_\infty = 39$ cm (FL).

Densities-at-length estimated by the model (from 1 cm to 39 cm FL) were further grouped to match the empirical size specification of Bonaire surveys (fish assigned to 5 cm classes, designated as 0–4 cm, 5–9 cm, and so on). The smallest size class (0–4 cm) was excluded from the fitting procedure because the detection of very small fish can be severely biased by visual census (23, 24). Moreover, the abundance of fish smaller than 5 cm cannot be represented with three months' growth increments. Since parrotfishes are homogeneous in shape (17), we also established a general length-weight relationship of the type $W = a\,L^{\,b}$ based on published estimates of parameters a and b available for twelve Caribbean parrotfishes (25–30). The strong interdependence of the two parameters (31, 32) was demonstrated by a highly significant ($N = 31$, $R^2 = 0.99$) regression of Log a over b (Fig. S1*B*):

$$\text{Log } a = -3.28\, b + 5.92 \qquad \textbf{[S7]}$$

Setting $b = 3$ [i.e., isometric growth (32)] provided a robust estimate of $a = 0.0198$ that can be used routinely to calculate the biomass of any Caribbean parrotfish from density-at-length data following:

$$W = 0.0198\, L^{\,3} \qquad \textbf{[S8]}$$

Biomasses were expressed in kg per hectare which is a relevant unit for fishery-oriented stock assessments.

We arbitrary fixed the value of parameter α_{sen} to 10^{-8} assuming mortality due to senescence is negligible at recruitment (i.e., compared to mortality due to predation). The other three mortality parameters (α_{pred}, β_{pred} and β_{sen}) and recruitment rate r (i.e., the number of 1-cm fish added to the population) were determined by optimizing model predictions of fish densities relative to those observed in Bonaire. Here we allowed fish to recruit at every time step because the reproductive activity of the stoplight parrotfish in Bonaire is persistent throughout the year (16). Specifically, the optimum combination of these four model parameters was identified by minimizing the negative log of the multinomial likelihood function LL of any particular observation j (2):

$$\mathrm{LL}_j\left(n_{ij} \mid r\ ,\ \alpha_{pred}\ ,\ \beta_{pred}\ ,\ \beta_{sen}\right) = \sum_{i=1}^{7} n_{ij}\ \log\ \frac{\hat{n}_i}{\sum_{i=1}^{7} \hat{n}_i} \qquad \textbf{[S9]}$$

where n_{ij} is the density of parrotfish observed in length class i in the sample j and $\hat{n}_i$ the density in length class i as simulated by the model at equilibrium. A sampled observation was a density-at-length vector (5-cm length classes) for a given time period and habitat (depth 6–12 m), averaged over two replicates and two observers. Although the available data represented four time periods (Dec. 1989, Mar. 1990, June 1990 and Jan. 1992), we selected only the first, third and last surveys in order to increase independence among observations (at least 6 months between two sampling periods). This resulted in six averaged size distributions, with their joint log-likelihood calculated as the product of the separate log-likelihoods combined with a penalty term:

$$\mathrm{LL}\left(n_{ij} \mid r\ ,\ \alpha_{pred}\ ,\ \beta_{pred}\ ,\ \beta_{sen}\right) = \prod_{j=1}^{6} \mathrm{LL}_j + penalty \qquad \textbf{[S10]}$$

The penalty term was introduced to constrain the optimization routine since recruitment rate and mortality of early-stage fish have compensatory effects on population abundance, thereby generating an infinite number of solutions for similar model fits: strong mortalities at small lengths will always compensate for high recruitment rates, and vice versa. This was overcome by simultaneously forcing (i) the sum of the simulated densities to equal the observed mean total and (ii) the mortality of settlers to equal an empirical estimate of 97% loss observed on *Sparisoma* spp. in Barbados within 3 months following settlement (11). Specifically, the penalty term was designed as follow:

$$penalty = \lambda_1 \left(\sum_{i=1}^{7} \bar{n}_i - \sum_{i=1}^{7} \hat{n}_i \right)^2 + \lambda_2 \left(s_{recruit} - 0.03 \right)^2 \qquad \textbf{[S11]}$$

where $s_{recruit}$ is the survival of recruit over a 3-month time step at equilibrium, and λ_1 and λ_2 are weighting terms arbitrary set to 1,000 and 50, respectively.

All minimizations were performed using the global search solver of the MATLAB optimization toolbox (33). A burn-in period of 20 years was applied to let the density-at-length vector approaching equilibrium. Likelihood profiles were then computed to estimate percentile confidence intervals (2) around parameters values for r, α_{pred}, β_{pred} and β_{sen} (Fig. S1*C*). The likelihood profile of a given parameter was built by optimizing the joint log-likelihood for incremental values of that parameter with all the other parameters being allowed to vary. The generated distribution of likelihoods was divided by their sum so that the cumulative distribution of standardized likelihoods equals one. The corresponding 95% confidence interval (CI) was then estimated by finding the parameter range that encompassed the central 95% of that distribution. Parameter CIs were consequently used to draw stochastic simulations by generating a random value for every parameter at every time step. The growth coefficient K was kept constant during stochastic simulations as variability in growth increments is already incorporated in the growth transition matrix. A total of six stochastic simulations were run to match the number of quadrats surveyed between December 1989 and January 1992. Predicted densities and biomasses at length and the instantaneous rate of adult mortality were retained at 20 years (i.e., the end of the burn-in period). Here, an "adult" stoplight parrotfish was defined based on a body length ≥ 15 cm FL, which roughly corresponds to the minimum size of 2 year old stoplight parrotfishes (17). Instantaneous mortality (yr^{-1}) of adults was calculated as:

$$z_{adults} = -\,\mathrm{Log}\,(s_{adults}) \qquad \textbf{[S12]}$$

where s_{adults} is the cumulative survivorship of fish ≥ 15 cm estimated for a one-year equivalent step. Due to high variations from one step to another during stochastic simulations, the actual estimate of adult mortality for each simulation was calculated by averaging adult mortality over the last year of that simulation. Bootstrapped 95% CIs were calculated for all model outputs and Bonaire observations based on 1000 samples.

At equilibrium, for the specified growth parameters (Table S1*A*), the demographic model reproduced well the size distribution of the stoplight parrotfish observed in Bonaire (see Fig. 1*A*). This close fit was conditional to an optimum value of 5.2 ind.100 m^{-2} (every 3 months) for settlement r, with a 95% CI largely skewed to the right (2.5–12.5 ind.100 m^{-2}, Fig. S1*C*). This strong asymmetry was generated by confounding effects of recruitment and juvenile mortality (driven by parameter α_{pred}), whereby different combinations of these two parameters produced a similarly good fit. Specifically, a good fit could be obtained with high recruitment rates when compensated by high mortality rates of juveniles. Such a large 95% CI for r caused excessive

fluctuations of population abundance during stochastic simulations, especially when parameters r and α_{pred} simultaneously took non-compensatory values, i.e., high recruitment rates followed by minimal mortality of juveniles. While in our simulations each random parameter value is generated independently, in nature, however, mortality of fish settlers is often density-dependent (8, 34) so that a peak of recruitment is likely to be dissipated by strong predation mortalities. To overcome the simultaneous generation of high recruitment and low mortality of juveniles, and therefore reduce the variability of the predicted density-at-lengths, each likelihood profile was approximated by a normal distribution centred on the optimum parameter value, with the *normal CI* matching the *likelihood-based CI* only at the 95% cut-off that is closer to the optimum value (see results in Fig. S1*C*). This pragmatic approach led to a restrained 95% CI for settlement (2.5–8.0 ind.100 m^{-2}). A normal approximation of parameter likelihood also simplifies the implementation of parameter stochasticity; random parameter values are generated at every iteration of the model from truncated normal distributions, so that every parameter value sits within its estimated normal 95% CI and not beyond. As a result, stochastic simulations produced fluctuations in density-at-lengths (see Fig. 1*A*), total density and total biomass (Fig. S1*D*) that were of similar magnitude to those observed among the Bonaire samples.

The instantaneous rate of adult mortality z_{adults} predicted by the model fluctuated between 0.34 and 0.41 yr^{-1} among simulations, with an average value of 0.37 yr^{-1} in the range of empirical estimates at low fishing levels [0.24–0.39 yr^{-1}, (17)]. Note that the extent of these fluctuations is dependent on the temporal window (one year) over which adult mortality was averaged within each simulation. Using the same survey data, van Rooij and Videler (9) calculated size-specific rates of natural mortality from growth rates estimated by mark-recapture. While they used a more sophisticated model integrating fish length, sex and social status (territoriality) in males, their mortality estimates compared very well with those estimated by the present model (see Fig. 1*B*). Overall, this indicates that a demographic model ignoring sex and social status is sufficient to represent the dynamics of the population size structure of the stoplight parrotfish.

The detailed body length distribution based on 1-cm size bins (Fig. S1*E*) showed irregularities in the distribution of small fish due to the chosen time step (3 months). Fish smaller than 5 cm FL are absent, whereas fish in the size range 6–15 cm have an uneven distribution that reflects a limited propagation of growth variability. While this structural bias could be overcome by spreading fish recruits in pre-specified length classes (3), it has minimal effects on the demographic outputs evaluated for fish larger than 15 cm. Moreover, because individual grazing rate increases substantially with body size (10, 35), we believe that an imprecise size distribution of juvenile abundance has negligible effects on the herbivore function delivered by the whole population.

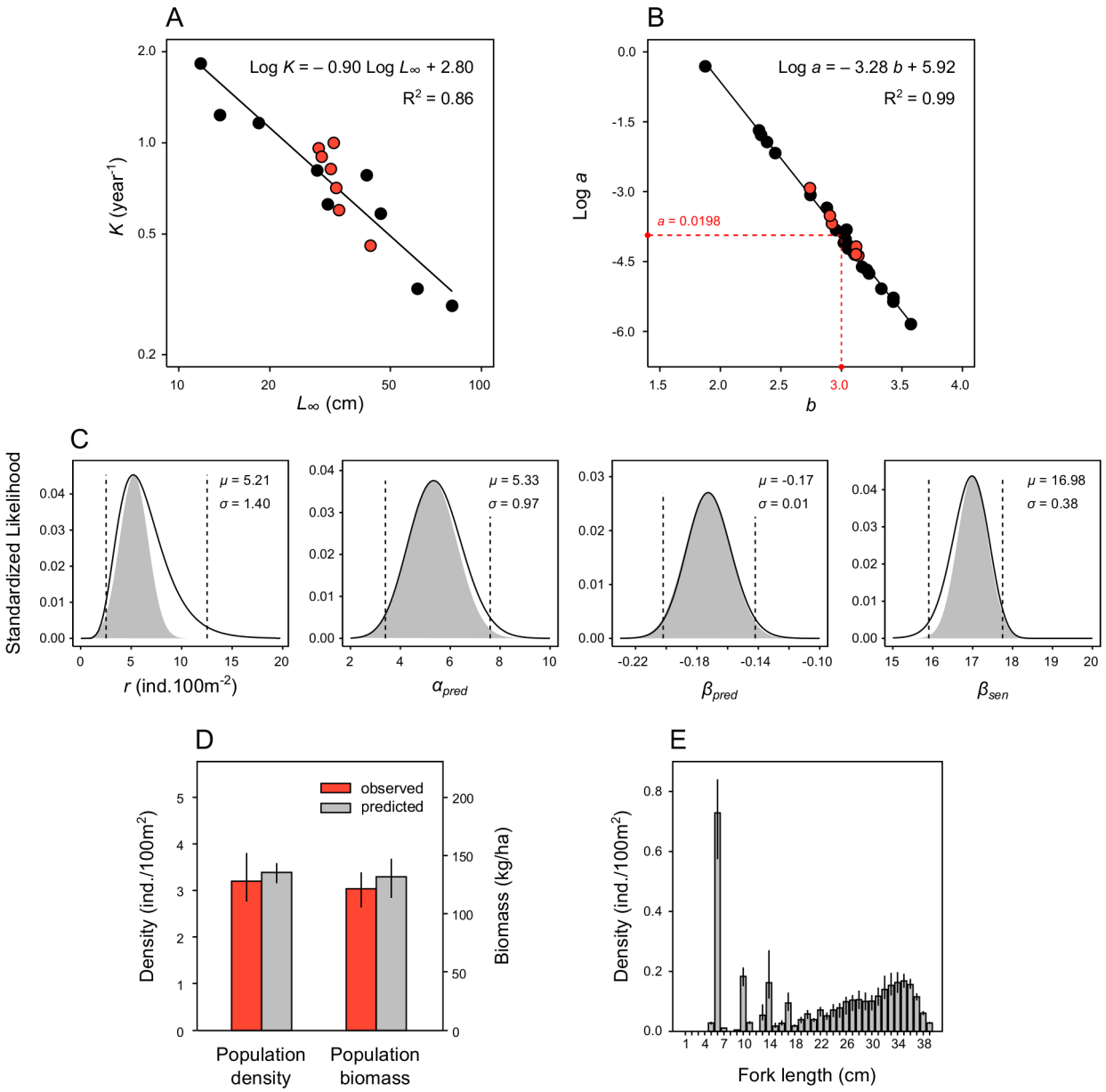

Fig. S1. Calibration of the demographic model of Caribbean parrotfishes. (*A*) Log-log relationship between asymptotic fork length L_∞ and Brody's growth coefficient K reported for 8 Caribbean parrotfishes (7, 17, 21, 22), including the stoplight parrotfish (red dots). (*B*) Published values of the length-weight conversion parameters a and b for 12 Caribbean parrotfishes (25–30) allowing derivation of a unique, family-wise length-weight relationship (Eq. S8). (*C*) Likelihood profiles of model parameters obtained by optimization against the observed size distributions of the stoplight parrotfish in Bonaire. Dotted lines represent 95% confidence limits. Grey areas represent the normal approximations centred on the optimum likelihood value (μ) with the corresponding standard deviation (σ) calculated by taking as a reference the closest confidence limit to the optimal likelihood. (*D*) Model predictions of density and biomass of the stoplight parrotfish (fish ≥ 5 cm FL) in Bonaire. (*E*) Density-at-length predictions at equilibrium in 1 cm increments. Error bars in (*D*) and (*E*) indicate 95% confidence intervals estimated by bootstrapping.

Table S1. Summary of parameter values used to model parrotfish populations

Population	L_∞ (cm)	K (year^{-1})	r (ind/100 m^2)	α_{pred}	β_{pred}	α_{sen}	β_{sen}
(A) Bonaire (6–12m)							
S. viride	39	0.62	**5.21**	**5.33**	**-0.173**	1e-8	**16.98**
(B) Bermuda (9–12m)							
S. viride	38	0.63	**3.47**	5.33	**-0.231**	1e-8	16.98
S. aurofrenatum	30	0.78	**5.55**	5.33	-0.231	1e-8	16.98
S. vetula	38	0.63	**4.16**	5.33	-0.231	1e-8	16.98
S. taeniopterus	34	0.70	**5.90**	5.33	-0.231	1e-8	16.98
S. iseri	28	0.83	**2.78**	5.33	-0.231	1e-8	16.98
(C) Bonaire (0.3–22m)							
S. viride	40	0.60	6.00	5.33	-0.173	1e-8	16.98
S. aurofrenatum	25	0.92	8.34	5.33	-0.173	1e-8	16.98
S. vetula	40	0.60	9.54	5.33	-0.173	1e-8	16.98
S. taeniopterus	29	0.80	7.56	5.33	-0.173	1e-8	16.98
S. iseri	27	0.86	8.28	5.33	-0.173	1e-8	16.98

Values in bold were determined by fitting model outputs to observed data. Parameter K was estimated from asymptotic length L_∞ using Eq. S6, with L_∞ approximated by the maximum length (FL) observed over the corresponding survey. Rates r, α_{pred} and α_{sen} are given for a three month time step. Recruitment r in Bermuda only occurred at one of every four steps. Recruitment of parrotfish populations in the depth range 0.3–22 m was estimated based on observed juvenile fish densities and a constant ratio of juvenile to recruit abundance across species; this ratio was determined using the stoplight parrotfish population of the depth stratum 6–12 m as a reference.

Sensitivity analysis. Model sensitivity to the parameters K, r, α_{pred}, β_{pred} and β_{sen} was investigated by measuring the effect of changing parametrization on four critical model outputs evaluated at equilibrium: (i) total abundance of the stoplight parrotfish population, (ii) average body length of adults, (iii) population biomass and (iv) instantaneous mortality of adults. The analysis was performed with the deterministic model by iterating the value of each parameter within its estimated 95% CI, while all other parameters were kept constant. Hence, parameter variations reflected the actual range of variability those parameters are subject to during stochastic simulations.

Results of the sensitivity analysis showed that mortality due to predation had the strongest effect on model outputs (Fig. S2). Low values for α_{pred} and β_{pred} generated disproportionally high

population densities and biomasses by, respectively, decreasing mortality rate per se and reducing the range of body lengths exposed to predation. High values for β_{pred} also strongly affected the instantaneous rate of adult mortality by extending predation losses to sizes well beyond 15 cm. By comparison, β_{sen} had a much lower effect on adult mortality because senescence essentially applies to a very limited number of size classes (the largest ones). For this reason, changes in mortality due to senescence mostly affected the average size of adults. Parameters K and r had both similar magnitude effects on fish density and biomass. Faster growth rates allow fish to escape predation quicker thus enhancing population abundance, whereas high recruitment rates translate to greater population sizes in the absence of density-dependent mortality. Slow growth rates had a disproportionate effect on the average size of adults by reducing the transition rate between length classes when fish become large. Mortality and average size of adults were insensitive to variations in recruitment rate.

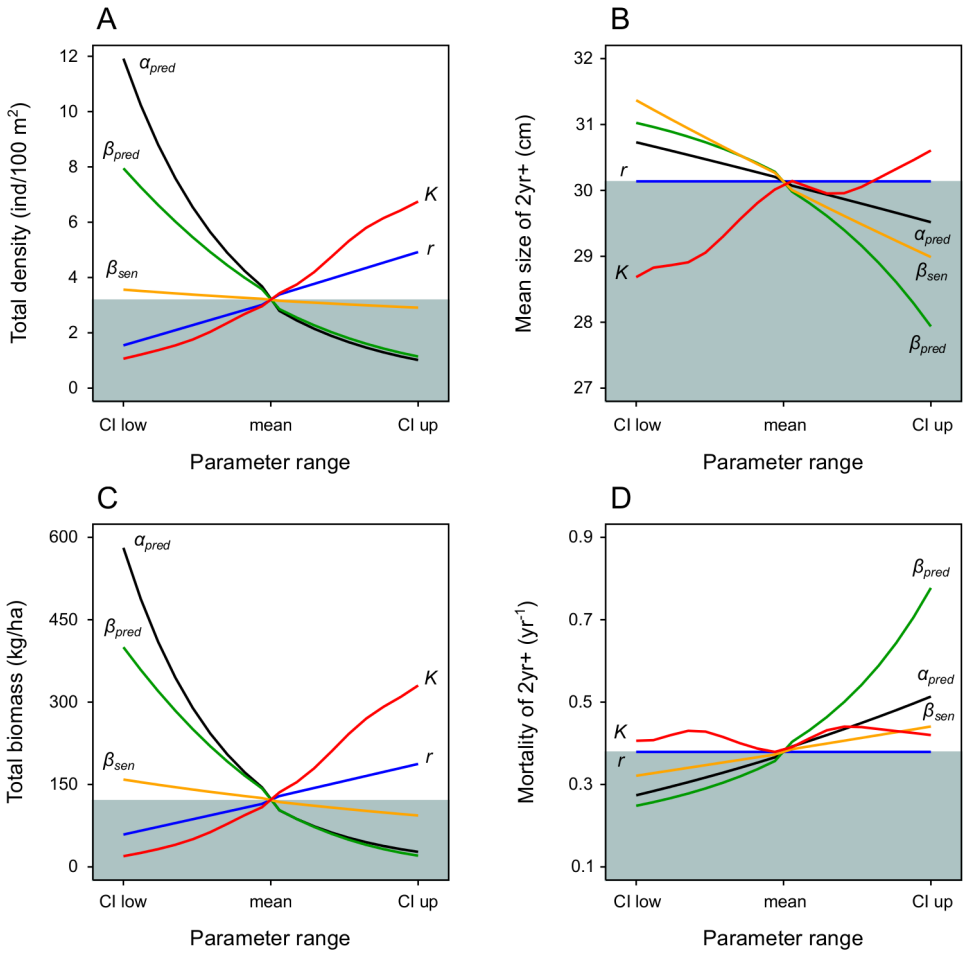

Fig. S2. Sensitivity of modeled stoplight parrotfish density (*A*), average body length of adults (*B*), population biomass (*C*) and adult mortality (*D*) to model parameters. Parameter values were varied between the lower (*CI low*) and upper (*CI up*) bounds of their normal 95% confidence interval. The grey area delineates the region where the output values are below the ones obtained with the optimal deterministic model, i.e., with all parameters fixed at their optimum value (*mean*).

Testing the model with independent data. Model performance was evaluated using a 12-yr fish survey data series (1991–2003) collected in Bermuda (36, 37) after the closure of a trap fishery. In April 1990, Bermuda banned the use of fish traps in response to alarming shifts in reef catch composition during the preceding decade (38, 39): parrotfishes previously discarded had become heavily targeted to compensate for significant declines in traditional food fishes (especially groupers). A long-term fish survey program was implemented in June 1991 to monitor the ecological effects of the fish trap ban on reef fish community structure (36). Surveys took place at four locations on the seaward side of the reef rim (depth range 9–12 m) that surrounds the Bermuda platform (36). Fish counts were performed using stationary point counts with a 7.5 m radius (40) and body length was visually estimated to the nearest cm (FL). While early assessments (1991–1993) did not reveal any significant trends for some parrotfish (including the stoplight parrotfish), later data (1994–1999, then 2003) clearly showed an increase in abundance and body length for most parrotfish species, resulting in a remarkable rise in parrotfish biomass (37).

We tested the ability of the model to reproduce the recovery of the stoplight parrotfish with minimal yet realistic parameter changes from the calibrated model. First, we assumed that settlement rate r would be much lower in Bermuda compared to Bonaire, because the geographical isolation of Bermuda restricts the replenishment of reef fish populations to local spawning (41). Mortality due to predation was also expected to be lower in Bermuda because most fish predators were depleted by decades of high fishing pressure (39). We only reduced the rate of decay of parrotfish mortality with size (β_{pred}), considering that fishing would have essentially released predation on medium-sized parrotfish, and kept unchanged the mortality at recruitment (α_{pred}) and parrotfish senescence (Table S1*B*). Parameters r and β_{pred} were modified within realistic boundaries until an acceptable agreement was visually found between the modeled trajectories of fish density and biomass and the observed trends. This fitting procedure was preferred over more precise parameter optimizations given the absence of recruitment and mortality data to corroborate the accuracy of parameter estimates.

We selected the observations made by the only one diver who took part to the entire survey, yielding a total of 1,125 point counts. Fish density was standardized to 100 m^2 and binned by size following the length-class scheme adopted in Bonaire as described above. Densities-at-length were averaged per periods of three months (27 survey periods with at least one site and eight counts per site) and converted into biomasses using Eq. S8. Asymptotic length L_∞ was set to 38 cm FL, which corresponded to the maximum length observed for the stoplight parrotfish during the entire survey. The growth coefficient K was estimated from L_∞ (Table S1*B*) using Eq. S6. Fishing mortality F was set to 0. Settlement was kept constant during the simulations; while isolated populations are prone to the existence of a stock-recruitment relationship, no significant increase in the numbers of post-larval recruits (< 5 cm) was observed over the recovery period in Bermuda (37). Because

recruitment in Bermuda is highly seasonal with a peak in summer for most reef fish (42), we allowed fish to recruit only at the third trimester (~July to September) of each simulated year. Specifically, seasonality in recruitment was evidenced by the recurrent observation of a peak of small fish density during the summer months (Fig. S3*A*). The absence of a seasonal peak during the first year of the time series was interpreted as a recruitment failure and has been therefore reproduced in our simulations (i.e., recruitment was prevented during the first year).

Stochastic simulations ($N = 200$) were initialized with density-at-lengths randomized from a normal distribution with mean and variance calculated over the first year of observations. Population abundance (Fig. S3*A*) and biomass (Fig. S3*B*) of the stoplight parrotfish more than doubled and reached a near equilibrium after approximately 7 years (i.e., by 1998). A good match between the modeled and observed trends and their associated variability was obtained for both population density and biomass, with a settlement rate of 3.5 ind.100 m^{-2} (at one of every four steps) and the mortality parameter β_{pred} lowered by 1/3 of its value in Bonaire (Table S1*B*). These adjustments produced a demographic equilibrium with a comparable size distribution (Fig. S3*C*) to the one observed on the stoplight parrotfish population during the last five years of the time series (presumed equilibrium). The resulting mortality rate of adults was 0.23 yr^{-1} on average, which logically was lower than the mortality rate estimated in Bonaire (0.37 yr^{-1} at equilibrium).

Testing the model with other parrotfish species. We next tested whether the model is able to reproduce the temporal patterns of the four other dominant parrotfish species of Bermuda after the cessation of trap fishing (36): the redband parrotfish, *Sparisoma aurofrenatum* (Valenciennes, 1840); the queen parrotfish, *Scarus vetula* Bloch & Schneider, 1801; the princess parrotfish, *Scarus taeniopterus* Lesson, 1829; the striped parrotfish, *Scarus iseri* (Bloch, 1789). We hypothesised that the model could predict their temporal trends by simply modifying the rate of recruitment previously adjusted for the stoplight parrotfish, without changing the parameters of mortality, thereby assuming a uniform predation mortality across parrotfishes at a given size (Table S1*B*). For each species, the growth coefficient K was estimated from L_∞ (maximum FL observed over the whole survey) using Eq. S6. As for the stoplight parrotfish, we allowed recruitment to occur at the third trimester of each simulated year. However, for the three *Scarus* species, surveys in the four sites of the reef rim revealed a consistent lack of juveniles compared to the two *Sparisoma* species. Patterns of association between juveniles and lagoonal patch reefs or nearshore habitats have been observed in Bermuda for a range of reef fish species, including *S. iseri* (42, 43). This suggests that some parrotfish may undertake ontogenetic migrations from shallow habitats to the reef, as reported in other Caribbean regions (44, 45). We therefore excluded the juvenile class of the three *Scarus* species [fish < 10 cm FL for *S. taeniopterus* and *S. iseri*, fish < 15 cm for *S. vetula*, (46)] from the representation of the modeled populations, thus implicitly assuming they recruit in other habitats and migrate to the outer rim reef at the transition to the adult initial phase.

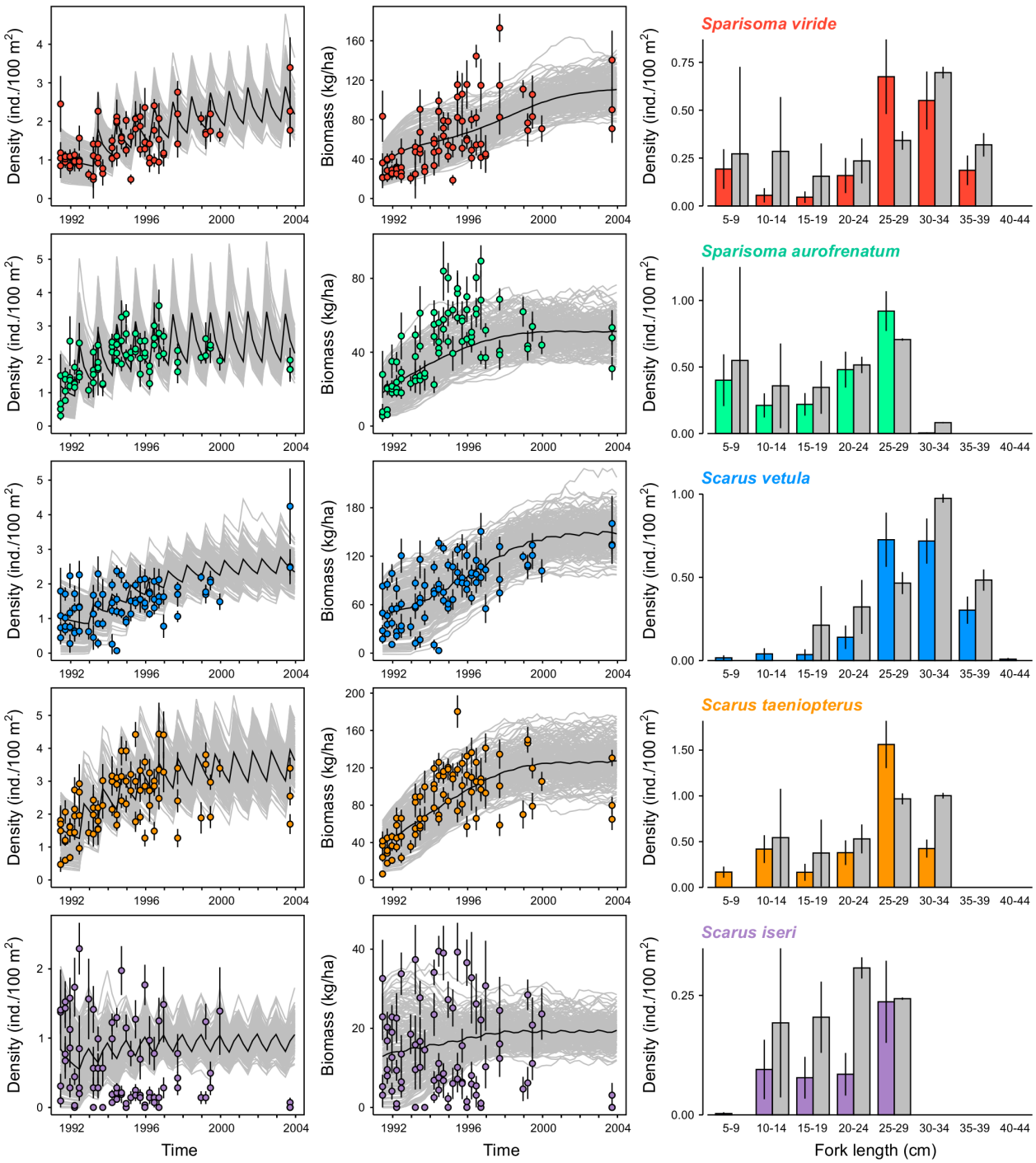

Fig. S3. Reconstructed trajectories of parrotfish population (fish ≥ 5 cm FL) density (*A*) and biomass (*B*) in Bermuda after the fish trap ban in April 1990. Dots represent the observed metrics at the four survey sites averaged over three-month periods, with error bars indicating the associated standard errors. Grey and black lines represent the individual (200 stochastic simulations) and average trajectories, respectively. (*C*) Observed (coloured bars) and predicted size distributions (grey bars) at the presumed equilibrium (Dec. 1998 – June 2003). Error bars represent, respectively, the standard deviations and errors of model estimates and observations.

Stochastic simulations ($N = 200$) were initialized with the average density-at-lengths observed during the first year. The average trajectory of both fish density (Fig. S3*A*) and biomass (Fig. S3*B*) was well reproduced for the redband, queen and princess parrotfish with credible values of recruitment (Table S1*B*). Variability among simulations also matched the observed variability of the two population metrics, and produced acceptable fits to the presumed equilibrial size distribution (Fig. S3*C*). However, simulating the temporal patterns of the striped parrotfish was challenged by the absence of significant trends on population density and biomass, which suggests that the striped parrotfish had been relatively unaffected by the trap fishery. Overall, changing the rate of recruitment was sufficient to reproduce the observed differences in demographic structure and dynamics among species of parrotfish.

Model generalization. Assuming that predation mortality is uniform across parrotfishes implies that differences in juvenile abundance are essentially due to differences in recruitment rate, especially for species having similar growth rate and similar habitat use across ontogeny. Specifically, such species are expected to exhibit the same ratio of density between juveniles and recruits. We tested this hypothesis using population censuses of the stoplight, redband, queen, princess and striped parrotfish, averaged over the full depth profile (0.3–22 m) surveyed at the Karpata site in Bonaire between Feb. 1989 and Jan. 1992 (46). Unlike Bermuda, the reef on the leeward side of Bonaire forms a narrow fringing reef that lacks back-reef habitats, so that ontogenetic migrations from outside of the modeled system can be considered minimal. In addition, the reef profile surveyed at the Karpata site included shallow habitats in which abundant juveniles ($\geq$ 5 cm) were found for all parrotfish species. We thus hypothesized that recruitment rate for all parrotfishes can be inferred from their observed juvenile density providing that this ratio is known for at least one species. Using the recruitment rate of the stoplight parrotfish estimated by the model at 6–12 m depths, recruitment for each parrotfish species was estimated by:

$$r_{species} = r_{viride} \times J_{species} / J_{viride} \qquad \textbf{[S13]}$$

where J denotes the average fish density observed in length classes 5-9 cm and 10-14 cm, a broad range of body lengths that is inclusive of all species juveniles [< 10 cm FL for *S. aurofrenatum*, *S. taeniopterus*, and *S. iseri*; < 15 cm for *S. viride* and *S. vetula*, (46)].

Model stochastic equilibrium was obtained after a 20-year burn-in period for each species (Table S1*C*) with the mortality parameters previously estimated for the stoplight parrotfish in Bonaire. As previously, the growth coefficient K was estimated from L_∞ using Eq. S6, assuming that L_∞ corresponds to the maximum length observed for each species. Equilibrial densities, biomasses and their associated variability were well predicted for all species (Fig. S4).

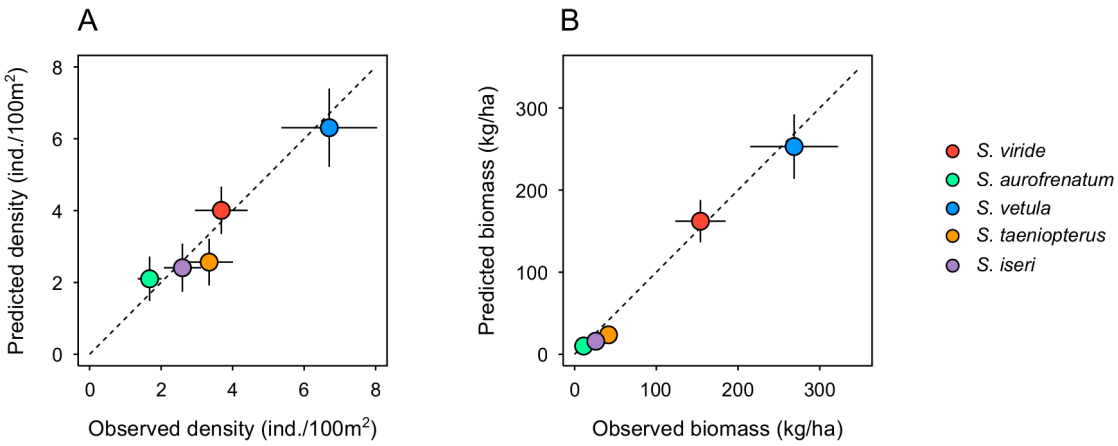

Fig. S4. Population (fish ≥ 5 cm FL) density (*A*) and biomass (*B*) of the five main parrotfish species as observed in the Karpata site of Bonaire in the depth range 0.3–22 m (46) and as predicted by the model at equilibrium, assuming recruitment rate is proportional to the observed juvenile (5–14 cm FL) fish density. Error bars represent, respectively, the standard deviations and errors for model estimates (200 stochastic simulations) and observations (28 quadrats).

While a reliable prediction of multiple population structure suggests that juvenile density is a good proxy of recruitment for parrotfish in Bonaire, the generality of this result is likely to be dependent on the proximity and functional link between reef populations and nursery habitats. As hypothesized in Bermuda, species that settle in nursery habitats will exhibit low reef abundances of juveniles if they recruit onto the reef at larger sizes. Moreover, the relationship between juvenile abundance and settlement rate would be different for nursery-dependent parrotfish because mortality of early-life stages is likely to be lower in nursery habitats. Clearly, specific assumptions about settlement and mortality rates are required when calibrating the model to populations that have strong functional links with nursery habitats (back-reefs, mangroves and seagrass beds).

Implementation of fishing. In Eq. S3, the instantaneous rate of fishing mortality F is size-dependent, assuming a knife-edge selection of size at first capture (i.e., selectivity p is 0 below the threshold size and 1 for every fish above) representative of reef fish trap selectivity (47). Considering that instantaneous fishing mortality and natural mortality take place simultaneously, the number of fish taken by the fishery in a given size class and during each time step was estimated *a posteriori* using the Baranov catch equation (2, 48):

$$\mathbf{c}_t = F\,\mathbf{p} \circ \mathbf{z}^{-1} \circ \mathbf{n}_t \circ [\,1 - \exp(-\mathbf{z})] \qquad \textbf{[S14]}$$

Catches in numbers for each parrotfish species were subsequently converted into weights using Eq. S8. Total catch was obtained by summing catch weights over all selected sizes and species and converted into a corresponding annual yield (kg/ha/year). Remaining fish densities were converted

into biomasses. In our analysis, stock biomass B (kg/ha) refers to this total biomass that survived natural and fishing mortality at the end of a time step. Harvest rate (%) was estimated during every time step as the proportion of exploitable stock biomass harvested by the fishery (i.e., the total catch divided by the exploitable stock biomass prior to mortality) and converted into a corresponding annual rate.

II. Model of instantaneous grazing rate of parrotfish

A model of parrotfish grazing (49) was used to calculate instantaneous grazing rates per individual for each species represented in the demographic model. The grazing model uses body length to predict the feeding rate and the size of bite scars of parrotfish at different life phase stages. Originally developed for the stoplight and queen parrotfishes in Bonaire (35, 46, 50), this grazing model was later extrapolated within the genera *Sparisoma* and *Scarus* with bite rates observed in Belize (49).

Bite rate, BR (bites.h^{-1}), decreases linearly with fork length L and is estimated as follows:

$$BR = phase \times [\ (\ \delta - \varphi \times L\ ) - offset\ ] \quad \textbf{[S15]}$$

where *phase* is a weighting factor accounting for the effect of life phase, δ and φ the parameters of the linear regression of feeding rate on body length and *offset* a correcting factor for each species (Table S2).

Bite size, BS (cm^2), increases with body length as follows (46):

$$BS = 5.257 \times 10^{-4} \times L^2 \text{ , for } \textit{Sparisoma} \text{ spp.} \quad \textbf{[S16a]}$$

$$BS = 4.013 \times 10^{-4} \times L^2 \text{ , for } \textit{Scarus} \text{ spp.} \quad \textbf{[S16b]}$$

Combining Eq. S15 and S16 with the density-at-length of each parrotfish species allows estimating species- and size-specific instantaneous grazing rates (GR) expressed as the percentage of the reef area (two-dimensional) grazed per hour:

$$GR_{s,i,t} = 100\% \times BR_{s,i} \times BS_{s,i} \times 10^{-4} \times n_{s,i,t} \times A^{-1} \quad \textbf{[S17]}$$

where $n_{s,i,t}$ is the density at length i of species s estimated at time step t and $A = 100$ m^2 the reference area of the model, representative of a standard field transect.

Table S2. Parameter values of the model of parrotfish feeding rate (Eq. S15)

Species	*phase* (J)	*phase* (IP)	*phase* (TP)	δ	φ	*offset*
S. viride	0.84	1.00	0.80	1089	17	56
S. aurofrenatum	0.84	1.00	0.80	1089	17	260
S. vetula	1.00	1.00	0.85	3329	33	0
S. taeniopterus	1.00	1.00	0.85	3329	33	1196
S. iseri	1.00	1.00	0.85	3329	33	1714

Life phases were categorised with the following size classes (46): for *S. viride* and *S. vetula*, juveniles (J): 1−14 cm, intermediate phase (IP): 15−29 cm, terminal phase (TP): 30−L_{inf} cm; for *S. aurofrenatum*, *S. taeniopterus* and *S. iseri*, J: 1−9 cm, IP: 10−19 cm, TP: 20−L_{inf} cm.

Species- and size-specific grazing rates were apportioned to three algal types (Table S3) based on observations of feeding preferences of different parrotfish species and life phases (49): (i) short algal turf, (ii) *Dictyota* and (iii) *Lobophora*. An instantaneous grazing rate for the whole parrotfish assemblage is finally calculated per algal type at every time step by summing the specific grazing rates across all species and body lengths. The overall grazing rate per algal type is a composite measure that depends on the relative abundance of different parrotfish species and size, and therefore integrates the complementarity in algal feeding among parrotfishes (51–54). Because some *Scarus* species (as opposed to *Sparisoma* spp.) have similar feeding preferences and bite rates than surgeonfishes (52, 53), this complementarity in feeding is representative of the diversity of feeding behaviours among functionally dominant Caribbean fish herbivores.

III. Spatially-explicit model of coral-reef dynamics

The model represents mid-depth (5–15 m) Caribbean forereefs and simulates the dynamics of coral colonies dispatched across a square lattice of 400 cells. The lattice grid has a toroidal structure so that every cell has continuous boundaries formed by 4 neighbouring cells. Each cell approximates 0.25 m^2 of reef and can be occupied by a mixture of living substrata including multiple coral colonies and algal patches so that interactions occur at colony scales as they do *in situ*. Corals are stylized by the cross-sectional, basal area of a hemispherical colony (cm^2). Two types of massive growth forms of corals are simulated: brooders (*BC*) and spawners (*SC*). Since white band disease has depleted populations of large, branching acroporid corals (55), these fast growing species are excluded. Reef algae are represented by patches of cropped algae (a mixture of coralline algae and short turf) and macroalgae (*Dictyota pulchella*, *Lobophora variegata*) whose size (cm^2) corresponds to the area of the colonised substrate. A number of cells are assigned to the class "ungrazable substrate" (e.g., sand) and prevented from any colonisation.

The model implements rates of recruitment, growth and mortality of corals and algae as well as their competitive interactions, calculated every six months. Corals grow in discrete increments and are subject to size-dependent mortality, resulting in three functional categories: *recruits* (size 1−60 cm^2), *juveniles* (61–250 cm^2), and *adults* (> 250 cm^2). Corals can recruit to individual patches of cropped algae but not macroalgae. Grazing affects all algal classes and always results in cropped algae. Grazing is spatially limited, so that only a proportion of the grazable substrate can be efficiently grazed over 6 months. If not grazed during 6 months, cropped algae gives rise to macroalgae which can overgrow corals. As a result, macroalgae increase once the availability of settlement space exceeds the grazing threshold (e.g., after severe coral mortality event). Competitive interactions between corals and macroalgae reduce the growth rate of each taxon and are the only process modeled to occur across cell boundaries (within a 4-cell von Neumann neighborhood). The spatial arrangement of elements within an individual cell is not explicit, but coral-coral competition can occur at intra-cellular scales. Finally, coral populations are subject to external disturbances (bleaching and hurricanes) which randomly affect their survival.

Table S3. Parrotfish feeding preferences as proportions of three algal types grazed by juveniles (J) intermediate phase (IP) and terminal phase (TP) individuals (49)

Species	Life phase	Turf	*Dictyota*	*Lobophora*
S. viride	J	1.00		
	IP	0.52	0.43	0.05
	TP	0.52	0.43	0.05
S. aurofrenatum	J	0.96	0.04	
	IP	0.42	0.54	0.04
	TP	0.42	0.54	0.04
S. vetula	J	1.00		
	IP	1.00		
	TP	1.00		
S. taeniopterus	J	1.00		
	IP	1.00		
	TP	1.00		
S. iseri	J	1.00		
	IP	1.00		
	TP	0.79	0.19	0.02

All model parameters are assumed to be constant rather than allowed to vary probabilistically. This approach avoids unnecessary variation from relatively well-established parameters and is consistent with other models of reef processes (56, 57). However, probabilistic rules and disturbance events generate stochasticity in model simulations. Model outputs include the cover (%) of each coral and algal species averaged over the stochastic simulations.

Initialisation. At the initial step, a number of cells are randomly designated as "ungrazable" until specified cover of ungrazable substrate of the grid lattice is achieved. The remaining (grazable) cells are randomly filled with coral colonies of different sizes until the sum of all colony sizes matches the specified coral cover for each species. Algal patches are created in a similar way by filling the remaining space in every grazable cell until their specified cover is reached.

Coral recruitment. Corals recruit to cropped algae because algal turfs are not heavily sediment-laden. Recruitment occurs at a size of 1 cm^2. Recruitment rates are based on pre-disturbance observations at Glovers Reef (58): 2 and 0.2 recruits per 0.25 m^2 of cropped algae for *BC* and *SC*, respectively.

Coral growth. Coral growth is modeled as lateral extension (radius increment per 6 month interval): *BC* have a lateral extension rate of 0.8 $cm.yr^{-1}$ and *SC* grow slightly faster at 0.9 $cm.yr^{-1}$ [based on median rates (59–63) for *Porites astreoides*, *Porites porites*, *Siderastrea siderea*, *Orbicella annularis*, *Colpophyllia natans* and *Agaricia agaricites*].

Coral reproduction. Coral reproduction is not explicitly modeled within the lattice, but rather the model assumes constant rate of coral recruitment from outside the reef (i.e., no stock-recruitment dynamics).

Colonization of cropped algae. Cropped algae arises (i) when macroalgae are grazed and (ii) after all coral mortality events (64) except those due to macroalgal overgrowth (see coral-algal competition below).

Colonization and vegetative growth of macroalgae. If not grazed during 6 months, cropped algae gives rise to *Dictyota* and *Lobophora*. Macroalgal rise is modeled for both species using a logistic growth function parametrized with empirical data (65, 66):

$$MA\ (t) = \frac{K_{MA} \times MA_0}{MA_0 + \left(K_{MA} - MA_0\right)\ \exp\ \left(-r_{MA} \times t\right)} \qquad \textbf{[S18]}$$

where $MA(t)$ is the cover (%) of macroalga (i.e., *Dictyota* or *Lobophora*) at a given time step, K_{MA} is the carrying capacity (48.8 and 100 for *Dictyota* and *Lobophora*, respectively), MA_0 the initial condition (1.33 and 0.33) and r_{MA} the instantaneous growth rate (4.37 and 0.59) for exposed reefs (windward). *Dictyota* always overgrows *Lobophora.*

Wave exposure. Wave exposure (i.e., "windward" or "leeward") affects algal productivity: growth rate of *Dictyota* on leeward reefs is 43% that of windward (67).

Season. Season (i.e., "summer" or "winter") alternates with every 6-month iteration of the model. *Dictyota* has a null cover in winter according to the die-back observed at Glovers Reef, Belize (67).

Competition between corals. Coral growth is constrained by the space currently available in a cell, so that competition between corals occurs when the cumulative potential growth exceeds available space. In that case, free space is shared between all coral colonies proportionally to their growth potential (size increment). This reflects the ability of faster/larger colonies to overtake slower/smaller colonies, as growth potential depends both on extension rate and current colony size.

Competition between corals and cropped algae. Corals always overgrow cropped algae (64).

Competition between corals and macroalgae: reduction of coral growth rate. The growth rate of recruits (1–60 cm^2) is set to zero if the local cover of macroalgae ($D + L$) > 80%, and reduced by 70% if macroalgal cover lies between 40% and ≤ 80% (68). Growth rate of larger corals (area > 60 cm^2) is reduced by up to 90% if macroalgal cover exceeds 40% (69), implemented as a step function.

Competition between corals and macroalgae: macroalgal overgrowth. Limited direct overgrowth of coral by macroalgae can occur. The macroalgal overgrowth of a living coral i ($O_{i \to M}$ in cm^2) results in partial mortality of the colony and is calculated as:

$$O_{C \to M} = MA_{5cells} \times P_i \times a_{MA,i} \qquad \textbf{[S19]}$$

where MA_{5cells} is the proportion of macroalga (i.e., *Dictyota* or *Lobophora*) in the focal cell and the von Neumann 4-cell neighborhood, P_i is the perimeter (cm) of the living coral colony i and $a_{MA,i}$ the average overgrowth (cm) of i due to the macroalga per cm length of coral edge.

Nugues and Bak (70) found that the average overgrowth of Agaricia and Porites (*BC1*) by *Lobophora* was 8 cm^2 per annum across a ~7 cm length of coral edge. This translates to $a_{L,i}$ = 0.57 cm per cm length of coral edge in each 6 month time step of the model. Values of $a_{L,i}$ for other corals were: *BC2* = 0.11, *SC1* = 0.11, *SC2* = 0.07. Note they did not find significant effects of *Lobophora* on all coral species studied. Whilst the correct interpretation of their data, the published results strongly suggest that an effect does exist and that a larger sample size may well have resulted in significant differences. Other studies have found negative effects of macroalgae on both massive (69) and branching corals (71).

Lirman (69) found no direct overgrowth of brooders by *Dictyota* but an overgrowth of 0.25 – 0.43 cm^2 $month^{-1}$ per cm length of coral edge on *Orbicella faveolata*. The lowest value of this range (no herbivory exclusion) translates to $a_{D,i} = 1.5$ cm for a 6 month time step and was applied to *SC1* and *SC2*.

Competition between corals and macroalgae: effect of corals on macroalgae. The probability with which macroalgae spread vegetatively over cropped algae, $P_{A \rightarrow M}$, is reduced by 25% when at least 50% of the local von Neumann neighborhood includes coral (64, 72):

$$P_{A \rightarrow M} = 0.75 \times MA_{5cells} \text{ , if } C_{5cells} \geq 0.5 \quad \textbf{[S20a]}$$

$$P_{A \rightarrow M} = MA_{5cells} \text{ , if } C_{5cells} < 0.5 \quad \textbf{[S20b]}$$

where C_{5cells} is the proportion of corals in the focal cell and the 4-cell von Neumann neighbourhood.

Partial-colony mortality of corals. Partial mortality is colony size-dependent, following empirical observations from Curaçao before major bleaching or hurricane disturbances (73). State variables reported in literature were converted to dynamic variables using least squares optimization until the equilibrial state in the model matched observed data. Partial mortality is implemented using the two equations below, where P_{pm} is the probability of a partial mortality event, A_{pm} is the area of tissue lost in a single event, and x is the size (planimetric area) of the coral in cm^2 before shrinkage:

$$P_{pm} = 1 - [\ (88.9 - 11.2 \text{ Log } x) / 100\ ] \quad \textbf{[S21]}$$

$$\text{Log } (A_{pm} \times 100) = -2.9 + 1.59 \times \text{Log } x \quad \textbf{[S22]}$$

Whole-colony mortality of juvenile and adult corals. Incidence of mortality (74) in juvenile corals (60–250 cm^2) is implemented as 2% per time interval (~ 4% per annum), halved to 1% (2% per annum) for mature colonies (> 250 cm^2). These levels of mortality occur in addition to macroalgal overgrowth (see above).

Parrotfish predation on coral recruits. Instantaneous whole-colony mortality occurs from parrotfish predation at a rate of 15% each 6-month iteration of the model (68). Predation is confined to small corals of planimetric area ≤ 5 cm^2, based on Meesters et al. (73) where between 60% and 95% of bite-type lesions were of this size.

Herbivory. Parrotfishes are the dominant herbivores on mid-depth Caribbean forereefs (75–78). All parrotfish species graze algal turfs (Table S3) and in doing so constrain the colonisation and vegetative growth of macroalgae. Direct removal of macroalgae occurs through the grazing of larger sparisomid species (up to 50% of bites in *S. viride*, Table S3). Because the model has a discrete time scale of six months, it does not capture the rapid turnover of algae resulting from continuous algal production and instantaneous grazing. Rather, what is required is an estimate of the net impact of grazing over a 6-month period: the surface area of the reef that is grazed sufficiently often that algae are maintained in a cropped state. Empirical and experimental studies have suggested that this net grazing impact (*GI*) may be limited to 30–40% of the reef substratum (49, 79, 80).

Fishing affects the instantaneous grazing rate of the parrotfish assemblage (Eq. S17), which occurs on a scale of seconds to minutes. Assuming this shift in grazing would hold linearly over a six month period, *GI* was adjusted in proportion to the changing instantaneous grazing rate, from a maximum value of 40% for an unfished reef area (80). At every time step, *GI* per algal type translates into a grazed algal surface (cm^2) based on the current surface area of the reef substrate. Parrotfish distribution is assumed to be homogeneous across the reefscape because the entire reef lattice falls within a continuous distribution of territories for each parrotfish species (81). For the larger-bodied species like *S. viride*, the model represents a single territory so the fish has equal access throughout; for the smaller-bodied species, like *S. iseri*, the reef constitutes up to 16 territories but these form a continuous set of adjacent territories on the reef (81). Grazing is thus implemented randomly across the reef (i.e., each grazable cell has an equal chance to be grazed) until the required amount of algal surface is totally consumed. If insufficient food exists, the fish switch prey to the next most favoured food item.

Hurricane impact on juvenile and adult corals: colony dislodgement. Whole-colony mortality (dislodgement) of live coral colonies > 60 cm^2 is modeled as a function of colony size and storm strength (82). For category 5 hurricanes, whole-colony mortality P_{hur} was represented using a quadratic function where x is the cross-sectional basal area of the colony in cm^2 (74, 83):

$$P_{hur} = -3 \times 10^{-7}\ x^2 + 7 \times 10^{-4}\ x + 0.0551 \qquad \textbf{[S23]}$$

Small colonies avoid dislodgement due to their low drag. Intermediate-sized corals have greater drag and are light enough to be dislodged, whereas large colonies are heavy enough to prevent dislodgement. For other hurricane categories, this function was modified by lowering the peak by the predicted impacts of each category of storm relative to the impacts of a category 5 storm. These relative predicted impacts (category 1: 4.6%; category 2: 11.8%; category 3: 25.0%; category 4: 56.8%) were determined by a simple relationship between storm intensity (wind speed), wave height, and predicted dislodgement (84, 85). Details on these calculations can be

found in Edwards et al. (82).

Hurricane impact on mature corals (> 250 cm2): partial-colony mortality. The extent of partial mortality due to hurricane (M_{hur}) is modeled using a Gaussian distribution with mean and standard deviation dependent on storm strength (with maximum mean of 0.30 and standard deviation of 0.20 for a category 5 hurricane). Each value of M_{hur} represents the percentage of original colony tissue that is lost due to the hurricane. If $M_{hur} \leq 0$, there is no mortality. If $M_{hur} \geq 1$, the entire colony is lost (though this is a rare event). Data come from monitoring of impact of Hurricane Mitch in Belize (86).

Hurricane impact on coral recruits (1-60 cm2): scouring by sand. Scouring by sand during a hurricane causes 80% whole-colony mortality in small juvenile corals (58).

Hurricane impact on macroalgae. Hurricanes reduce the cover of macroalgae to 10% of its pre-hurricane level (86).

Whole-colony mortality due to bleaching. Whole-colony mortality was modeled as a function of the number of degree heating weeks (DHW) predicted for a given location and year. Data were taken from 1057 field surveys in the Caribbean, spanning the timeframe 4-Jun-2005 through 21-Jan-2006 (87). These data were collected during the most extensive coral bleaching event recorded in the greater Caribbean (87, 88). For each data pixel, Eakin et al. (87) calculated the DHW (°C weeks) values, and the date and value of the maximum DHW. The number of degree heating weeks is calculated by accumulating HotSpots greater than 1 that occur during a 12-week window, where a HotSpot is defined as the temperature above the monthly maximum, in the monthly climatology, for each grid cell (89). For observations taken before the date of the maximum DHW value for that pixel, the DHW value at the time of the observation was used as the measure of thermal stress; otherwise, the maximum DHW value was used.

Mortality of colonies was related to thermal stress experienced at a site. There was, however, significant variability in mortality with DHW. For predicted DHWs within the range experienced by sites in 2005 (DHW < 17), data from the window [DHW-1, DHW+1] to generate a distribution of mortalities, from which a value for mortality was drawn. For all windows centered on integer values (0-2 up to 16-18) the standard deviation of data within each window was calculated; these values were averaged to give an overall measure of variability. To enable simulation of thermal stress greater than that experienced in 2005 (DHWs ≥ 17), we used linear regression analysis to establish the relationship between DHW and colonies undergoing mortality because of bleaching, and sampled from the regression equation using its standard error.

Bleaching does not occur if a hurricane has occurred that year, assuming that hurricanes can cool reef waters below the bleaching threshold (87, 90). In addition, corals previously exposed to

elevated temperatures have a reduced risk (30%) of mortality due to bleaching [data from van Woesik et al. (91)]. The response of corals to successive bleaching events has not yet been monitored in the Caribbean. However, the fate of 12 Pacific coral species during a period in which two bleaching events occurred was monitored in Okinawa from 1998 to 2002 (91). No coral species monitored were common to both the Pacific and Caribbean and therefore we focused on the response of non-acroporid Pacific species that best compared with massive and encrusting morphology of most reef-building corals in the Caribbean. Population responses of *Porites lutea*, *Favia pallida* and *Favia favus* over six time periods (Sept 1998 to May 2002) were used to derive the proportion of corals that were resistant (no discernible bleaching), resilient (bleached and recovered) or killed as a result of each bleaching event. The proportion of coral colonies killed as a result of bleaching was lower for the second bleaching event for all three species. Averaging over these species, the risk of mortality because of the second event was approximately 30% of that due to the first event. Whilst the actual risk of mortality will vary with species and with thermal stress, it is assumed that the similar reduction in mortality risk could be applied to Caribbean corals in the model if they have been previously exposed to elevated temperatures.

Partial-colony mortality due to bleaching. Data on partial-colony mortality (92) was taken from 13 sites on the Belize barrier reef during the 1995 bleaching event (93). Tagged colonies (68 in total) were monitored from October 1995 to May 1996 and corals were ranked by condition (normal, pale, part bleached, bleached and partial mortality) following methods of CARICOMP (94) and Lang et al. (95). All tagged colonies experienced bleaching (as opposed to only 52% of all coral colonies in the surveyed area) and the data suggested that those tagged colonies may have been more severely bleached than the overall population. Taking this into account, 12% of all coral colonies were estimated to have undergone partial mortality by May 1996.

Data from Belize for *Orbicella* spp. and *Siderastrea siderea* showed that 7.4% of spawning corals underwent partial mortality. Similarly, averaging over *Agaricia tenuifolia* and *Porites spp.* gave 8.3% partial mortality for brooding corals. The probability of partial mortality during a bleaching event (DHW > 4) was thus modeled as 7% and 8% for brooders and spawners respectively. The extent of partial mortality was set at 30% of tissue area (92).

IV. Model assumptions and limitations

Although the use of a complex simulation model allows available scientific information to be integrated and inform predictions of resilience, any model has to make a number of simplifying assumptions. Here, we assume that coral populations are demographically open because the nature and scale of stock-recruitment relationships remain unknown for brooders and spawners (96). We also assume that no gradual adaptation to climate change takes place and that the response of

corals to bleaching is dominated by the intensity of acute thermal stress and not modified by acclimation. For example, the model ignores sub-lethal effects of chronic thermal stresses [e.g., reduced coral growth (97, 98)] and their potential synergies with coral bleaching mortality on reef resilience (99). Ocean acidification is not considered because spatial heterogeneity in its magnitude and effects remain unknown. Finally, the model assumes that urchins *Diadema* and branching acroporids are functionally extinct and will remain so in a near future (i.e., by 2030), although significant recovery of these two organisms across the Caribbean are likely to increase resilience (49, 100). In contrast, an increase in white band disease, perhaps under climate change, would worsen the outlook for reef resilience and require even lower harvest rates.

Parrotfish are important grazers on all but the shallowest of Caribbean reefs as they typically comprise more than 70%, often 90% of total herbivore biomass (78). There is considerable evidence that parrotfish grazing is a major control of macroalgae with studies coming from the whole Caribbean (78), and locally within Florida (51), the Bahamas (10), Belize (79, 101) and Bonaire (102). Other fish such as surgeonfishes (Acanthuridae) significantly contribute to the overall grazing intensity (51, 53, 54), especially on shallow reefs (<5m). A recent manipulative experiment of parrotfish grazing – that had no effect on surgeonfish – found that depletion of larger parrotfish led to massive macroalgal blooms, often reaching 80% algal cover (101).

External disturbances are assumed to have no direct impacts on parrotfish population structure. Direct mortalities of coral-reef fish caused by storms have been anecdotal and mostly confined to the shallowest parts of reefs (103). While some studies have reported storm-induced habitat shifts and disruptions in coral-reef fish behaviour (103–105), these effects did not last for longer than a few weeks. Moreover, detailed studies of parrotfish assemblages in a marine reserve in Belize revealed that both bleaching and hurricane events had no direct effect on parrotfish populations within a model time step (86).

While Bermuda arguably represents one of the most extreme case of a closed fish population in the Caribbean, no stock-recruitment relationship could be detected over a 12 year period, even though adult population size more than doubled for most parrotfish species (37). While we acknowledge that a constant recruitment rate is a simplifying assumption, it also offered the most parsimonious model because the recovery of parrotfish populations could be reproduced without requiring a stock-recruitment relationship. Specifically, the model demonstrated that a release of fishing mortality is itself enough to double fish abundance just because fish can live longer, which was corroborated by an increasing number of large fish in the survey. However, the assumption of parrotfish recruitment independent of adult stock should be revisited geographically for a range of species, and especially for fisheries where parrotfish have been considerably depleted by decades of overfishing.

The short-term impact of changes in available food (algae) for herbivores is not considered because where parrotfish population size has been tracked over a profound loss of coral in the Caribbean, no increase was observed within three years of a major disturbance that led to a rapid threefold loss of coral (86). While parrotfish biomass has been shown to decrease at very high levels of coral cover in the Pacific (106), such extreme coral covers are virtually absent from the Caribbean. While the simulated time-frame (15 years) may be long enough to observe negative impacts of coral mortality on the reef structural complexity [(107, 108) but see (109)] we assume that grazing intensity is robust to a loss of coral reef structure because the effect on parrotfish feeding is stabilised by opposing ecological processes (110). A modest loss of habitat complexity would usually result in a small reduction in parrotfish abundance. However, because parrotfish now graze over a smaller surface area (the reef is 'flatter'), the reduction in fish abundance is offset by the increase in grazing intensity that occurs as grazing area declines (110).

V. References

1. Sullivan PJ (1992) A Kalman filter approach to catch-at-length analysis. *Biometrics* 48(1):237–257.
2. Haddon M (2011) *Modelling and quantitative methods in fisheries* (CRC Press/Chapman and Hall, New York).
3. Punt AE, Huang T, Maunder MN (2013) Review of integrated size-structured models for stock assessment of hard-to-age crustacean and mollusc species. *ICES J Mar Sci* 70(1):16–33.
4. Nelson GA (2014) *fishmethods: fishery science methods and models in R* Available at: Available at http://CRAN.R-project.org/package=fishmethods. [Accessed January 14, 2016].
5. Chen Y, Hunter M, Vadas R, Beal B (2003) Developing a growth-transition matrix for the stock assessment of the green sea urchin (*Strongylocentrotus droebachiensis*) off Maine. *Fish Bull* 101(4):737–744.
6. Tolimieri N (1998) Effects of substrata, resident conspecifics and damselfish on the settlement and recruitment of the stoplight parrotfish, *Sparisoma viride*. *Environ Biol Fishes* 53(4):393–404.
7. Choat JH, Robertson DR (2002) Age-based studies. *Coral Reef Fishes: Dynamics and Diversity in a Complex Ecosystem*, ed Sale PF (Academic Press, San Diego, California, USA), pp 57–80.
8. Hixon MA, Webster MS (2002) Density dependence in reef fish populations. *Coral Reef Fishes: Dynamics and Diversity in a Complex Ecosystem*, ed Sale PF (Academic Press, San Diego, California, USA), pp 303–325.
9. van Rooij JM, Videler JJ (1997) Mortality estimates from repeated visual censuses of a parrotfish (*Sparisoma viride*) population: demographic implications. *Mar Biol* 128(3):385–396.
10. Mumby PJ, et al. (2006) Fishing, trophic cascades, and the process of grazing on coral reefs. *Science* 311(5757):98–101.
11. Vallès H, Kramer DL, Hunte W (2008) Differential effect of early post-settlement processes on the abundance of two concurrently settling coral reef fishes. *Proc 11th Int Coral Reef Symp Ft Lauderdale Fla*:335–339.
12. Hixon MA (1991) Predation as a process structuring coral reef fish communities. *The Ecology of Fishes on Coral Reefs*, ed Sale PF (Academic Press, San Diego), pp 475–508.

13. Almany GR, Webster MS (2006) The predation gauntlet: early post-settlement mortality in reef fishes. *Coral Reefs* 25(1):19–22.
14. van Rooij JM (1996) *Behavioural energetics of the parrotfish Sparisoma viride. Flexibility in a coral reef setting.* PhD dissertation (University of Groningen, The Netherlands). Available at: http://irs.ub.rug.nl/ppn/331416387. [Accessed January 14, 2016].
15. Bruggemann JH (1995) *Parrotfish grazing on coral reefs: a trophic novelty*. PhD dissertation (University of Groningen, The Netherlands). Available at: http://irs.ub.rug.nl/ppn/126795320. [Accessed January 14, 2016].
16. van Rooij JM, Kroon FJ, Videler JJ (1996) The social and mating system of the herbivorous reef fish *Sparisoma viride*: one-male versus multi-male groups. *Environ Biol Fishes* 47(4):353–378.
17. Choat JH, Robertson DR, Ackerman JL, Posada JM (2003) An age-based demographic analysis of the Caribbean stoplight parrotfish *Sparisoma viride*. *Mar Ecol Prog Ser* 246:265–277.
18. Hawkins JP, Roberts CM (2003) Effects of fishing on sex-changing Caribbean parrotfishes. *Biol Conserv* 115(2):213–226.
19. van Rooij JM, Bruggemann JH, Videler JJ, Breeman AM (1995) Plastic growth of the herbivorous reef fish *Sparisoma viride*: field evidence for a trade-off between growth and reproduction. *Mar Ecol Prog Ser* 122:93–105.
20. Pauly D (1998) Tropical fishes: patterns and propensities. *J Fish Biol* 53(Suppl. A):1–17.
21. Randall JE (1962) Tagging reef fishes in the Virgin Islands. *Proc Gulf Caribb Fish Inst* 14:201–241.
22. Paddack MJ, Sponaugle S, Cowen RK (2009) Small-scale demographic variation in the stoplight parrotfish *Sparisoma viride*. *J Fish Biol* 75(10):2509–2526.
23. Bozec Y-M, Kulbicki M, Laloë F, Mou-Tham G, Gascuel D (2011) Factors affecting the detection distances of reef fish: implications for visual counts. *Mar Biol* 158(5):969–981.
24. Willis TJ (2001) Visual census methods underestimate density and diversity of cryptic reef fishes. *J Fish Biol* 59:1408–1411.
25. Reeson P (1983) The biology, ecology and bionomics of the parrotfishes, Scaridae. *Caribbean Coral Reef Fishery Resources*, ed Munro J (ICLARM Studies and Reviews), pp 166–177.
26. Bouchon-Navaro Y, Bouchon C, Kopp D, Louis M (2006) Weight–length relationships for 50 fish species collected in seagrass beds of the Lesser Antilles. *J Appl Ichthyol* 22(4):322–324.
27. Claro R, García-Arteaga J (1994) Crecimiento. *Ecología de Los Peces Marinos de Cuba*, ed Claro R (Instituto de Oceanologia Academia de Ciencias de Cuba and Centro de Investigaciones de Quintana Roo (CIQRO), México), pp 321–402.
28. Bohnsack JA, Harper DE (1988) *Length-weight relationships of selected marine reef fishes from the southeastern United States and the Caribbean* (NOAA, National Marine Fisheries Service, Southeast Fisheries Center).
29. Paddack MJ, Cowen RK, Sponaugle S (2006) Grazing pressure of herbivorous coral reef fishes on low coral-cover reefs. *Coral Reefs* 25(3):461–472.
30. van Rooij JM, Videler JJ, Bruggemann JH (1998) High biomass and production but low energy transfer efficiency of Caribbean parrotfish: implications for trophic models of coral reefs. *J Fish Biol* 53(Suppl. A):154–178.
31. Kulbicki M, Guillemot N, Amand M (2005) A general approach to length-weight relationships for New Caledonian lagoon fishes. *Cybium* 29(3):235–252.
32. Froese R (2006) Cube law, condition factor and weight–length relationships: history, meta-analysis and recommendations. *J Appl Ichthyol* 22(4):241–253.

33. MathWorks Inc. (2012) *MATLAB. Release R2012a* (The MathWorks, Inc., Natick, Massachusetts).
34. Hixon MA, Carr MH (1997) Synergistic predation, density dependence, and population regulation in marine fish. *Science* 277(5328):946–949.
35. Bruggemann JH, Begeman J, Bosma EM, Verburg P, Breeman AM (1994) Foraging by the stoplight parrotfish *Sparisoma viride*. II. Intake and assimilation of food, protein, and energy. *Mar Ecol Prog Ser* 106:57–71.
36. Luckhurst BE (1994) A fishery-independent assessment of Bermuda's coral reef fish stocks by diver census following the fish pot ban–a progress report. *Proc Gulf Caribb Fish Inst* 46:309–323.
37. O'Farrell S, Harborne AR, Bozec Y-M, Luckhurst BE, Mumby PJ (2015) Protection of functionally important parrotfishes increases their biomass but fails to deliver enhanced recruitment. *Mar Ecol Prog Ser* 522:245–254.
38. Butler JN, Burnett-Herkes J, Barnes JA, Ward J (1993) The Bermuda fisheries: a tragedy of the commons averted? *Environment* 35(1):6–15:25–33.
39. Luckhurst BE, Ward JA (1996) Analysis of trends in Bermuda's fishery statistical database from 1975 to 1990 with reference to fishery management measures implemented during this period. *Proc Gulf Caribb Fish Inst* 44:306–324.
40. Bohnsack JA, Bannerot SP (1986) *A stationary visual census technique for quantitatively assessing community structure of coral reef fishes*.
41. Schultz ET, Cowen RK (1994) Recruitment of coral reef fishes to Bermuda: Local retention or long-distance transport? *Mar Ecol Prog Ser* 109:15–28.
42. Smith SR, de Putron S, Murdoch TJ, Pitt JM, Nagelkerken I (2013) Biology and ecology of corals and fishes on the Bermuda platform. *Coral Reefs of the United Kingdom Overseas Territories*, ed Sheppard C (Springer), pp 135–151.
43. Huijbers CM, Grol MGG, Nagelkerken I (2008) Shallow patch reefs as alternative habitats for early juveniles of some mangrove/seagrass-associated fish species in Bermuda. *Int J Trop Biol Conserv* 56:161–169.
44. Nagelkerken I, Dorenbosch M, Verberk W, de la Moriniere EC, van der Velde G (2000) Importance of shallow-water biotopes of a Caribbean bay for juvenile coral reef fishes: patterns in biotope association, community structure and spatial distribution. *Mar Ecol Prog Ser* 202:175–192.
45. Nagelkerken I, et al. (2002) How important are mangroves and seagrass beds for coral-reef fish? The nursery hypothesis tested on an island scale. *Mar Ecol Prog Ser* 244(2002):299–305.
46. Bruggemann JH, Van Kessel AM, Van Rooij JM, Breeman AM (1996) Bioerosion and sediment ingestion by the Caribbean parrotfish *Scarus vetula* and *Sparisoma viride*: implications of fish size, feeding mode and habitat use. *Mar Ecol Prog Ser* 134(1):59–71.
47. Mahon R, Hunte W (2001) Trap mesh selectivity and the management of reef fishes. *Fish Fish* 2(4):356–375.
48. Ricker WE (1975) Computation and interpretation of biological statistics of fish populations. *Bull Fish Res Board Can* 191:1–382.
49. Mumby PJ (2006) The impact of exploiting grazers (Scaridae) on the dynamics of Caribbean coral reefs. *Ecol Appl* 16(2):747–769.
50. Bruggemann JH, Kuyper MW, Breeman AM (1994) Comparative analysis of foraging and habitat use by the sympatric Caribbean parrotfish *Scarus vetula* and *Sparisoma viride* (Scaridae). *Mar Ecol Prog Ser* 112(1-2):51–66.
51. Burkepile DE, Hay ME (2008) Herbivore species richness and feeding complementarity affect

community structure and function on a coral reef. *Proc Natl Acad Sci USA* 105(42):16201–16206.

52. Burkepile DE, Hay ME (2010) Impact of herbivore identity on algal succession and coral growth on a Caribbean reef. *PLoS One* 5(1):e8963.
53. Burkepile DE, Hay ME (2011) Feeding complementarity versus redundancy among herbivorous fishes on a Caribbean reef. *Coral Reefs* 30(2):351–362.
54. Adam TC, Burkepile DE, Ruttenberg BI, Paddack MJ (2015) Herbivory and the resilience of Caribbean coral reefs: knowledge gaps and implications for management. *Mar Ecol Prog Ser* 520:1–20.
55. Aronson RB, Precht WF (2001) White-band disease and the changing face of Caribbean coral reefs. *Hydrobiologia* 460(1-3):25–38.
56. McClanahan TR (1995) A coral reef ecosystem-fisheries model: impacts of fishing intensity and catch selection on reef structure and processes. *Ecol Model* 80(1):1–19.
57. Langmead O, Sheppard C (2004) Coral reef community dynamics and disturbance: a simulation model. *Ecol Model* 175(3):271–290.
58. Mumby PJ (1999) Bleaching and hurricane disturbances to populations of coral recruits in Belize. *Mar Ecol Prog Ser* 190:27–35.
59. Maguire LA, Porter JW (1977) A spatial model of growth and competition strategies in coral communities. *Ecol Model* 3(4):249–271.
60. Highsmith RC, Lueptow RL, Schonberg SC (1983) Growth and bioerosion of three massive corals on the Belize barrier reef. *Mar Ecol Prog Ser* 13:261–271.
61. Huston M (1985) Variation in coral growth rates with depth at Discovery Bay, Jamaica. *Coral Reefs* 4(1):19–25.
62. Chornesky EA, Peters EC (1987) Sexual reproduction and colony growth in the scleractinian coral *Porites astreoides*. *Biol Bull* 172(2):161–177.
63. van Moorsel GWNM (1988) Early maximum growth of stony corals (Scleractinia) after settlement on artificial substrata on a Caribbean reef. *Mar Ecol Prog Ser* 50:127–135.
64. Jompa J, McCook LJ (2002) Effects of competition and herbivory on interactions between a hard coral and a brown alga. *J Exp Mar Biol Ecol* 271(1):25–39.
65. De Ruyter van Steveninck ED, Breeman AM (1987) Deep water populations of *Lobophora variegata* (Phaeophyceae) on the coral reef of Curaçao: influence of grazing and dispersal on distribution patterns. *Mar Ecol Prog Ser* 38:241–250.
66. Renken H (2008) *Macroalgal dynamics on Caribbean coral forereefs*. PhD dissertation (University of Exeter, UK. Available at: https://ore.exeter.ac.uk/repository/bitstream/handle/10036/41253/RenkenH.pdf?sequence=3. [Accessed January 14, 2016].
67. Renken H, Mumby PJ, Matsikis I, Edwards HJ (2010) Effects of physical environmental conditions on the patch dynamics of *Dictyota pulchella* and *Lobophora variegata* on Caribbean coral reefs. *Mar Ecol Prog Ser* 403:63–74.
68. Box SJ, Mumby PJ (2007) Effect of macroalgal competition on growth and survival of juvenile Caribbean corals. *Mar Ecol Prog Ser* 342:139–149.
69. Lirman D (2001) Competition between macroalgae and corals: effects of herbivore exclusion and increased algal biomass on coral survivorship and growth. *Coral Reefs* 19(4):392–399.
70. Nugues MM, Bak RP (2006) Differential competitive abilities between Caribbean coral species and a brown alga: a year of experiments and a long-term perspective. *Mar Ecol Prog Ser* 315:75–86.

71. Jompa J, McCook LJ (2002) The effects of nutrients and herbivory on competition between a hard coral (*Porites cylindrica*) and a brown alga (*Lobophora variegata*). *Limnol Oceanogr* 47(2):527–534.
72. De Ruyter van Steveninck ED, Van Mulekom LL, Breeman AM (1988) Growth inhibition of *Lobophora variegata* (Lamouroux) Womersley by scleractinian corals. *J Exp Mar Biol Ecol* 115(2):169–178.
73. Meesters EH, Wesseling I, Bak RP (1997) Coral colony tissue damage in six species of reef-building corals: partial mortality in relation with depth and surface area. *J Sea Res* 37(1):131–144.
74. Bythell JC, Gladfelter EH, Bythell M (1993) Chronic and catastrophic natural mortality of three common Caribbean reef corals. *Coral Reefs* 12(3-4):143–152.
75. Lewis SM, Wainwright PC (1985) Herbivore abundance and grazing intensity on a Caribbean coral reef. *J Exp Mar Biol Ecol* 87(3):215–228.
76. Morrison D (1988) Comparing fish and urchin grazing in shallow and deeper coral reef algal communities. *Ecology*:1367–1382.
77. Steneck RS (1994) Is herbivore loss more damaging to reefs than hurricanes? Case studies from two Caribbean reef systems (1978–1988). *Proceedings of the Colloquium on Global Aspects of Coral Reefs: Health, Hazards and History*, ed Ginsburg RNE, pp 220–226.
78. Williams I, Polunin N (2001) Large-scale associations between macroalgal cover and grazer biomass on mid-depth reefs in the Caribbean. *Coral Reefs* 19(4):358–366.
79. Williams ID, Polunin NV, Hendrick VJ (2001) Limits to grazing by herbivorous fishes and the impact of low coral cover on macroalgal abundance on a coral reef in Belize. *Mar Ecol Prog Ser* 222:187–196.
80. Mumby PJ, Hastings A, Edwards HJ (2007) Thresholds and the resilience of Caribbean coral reefs. *Nature* 450(7166):98–101.
81. Mumby PJ, Wabnitz CC (2002) Spatial patterns of aggression, territory size, and harem size in five sympatric Caribbean parrotfish species. *Environ Biol Fishes* 63(3):265–279.
82. Edwards HJ, et al. (2011) How much time can herbivore protection buy for coral reefs under realistic regimes of hurricanes and coral bleaching? *Glob Change Biol* 17(6):2033–2048.
83. Massel SR, Done TJ (1993) Effects of cyclone waves on massive coral assemblages on the Great Barrier Reef: meteorology, hydrodynamics and demography. *Coral Reefs* 12(3-4):153–166.
84. Madin JS, Connolly SR (2006) Ecological consequences of major hydrodynamic disturbances on coral reefs. *Nature* 444(7118):477–480.
85. Madin JS, Black KP, Connolly SR (2006) Scaling water motion on coral reefs: from regional to organismal scales. *Coral Reefs* 25(4):635–644.
86. Mumby PJ, Foster NL, Fahy EAG (2005) Patch dynamics of coral reef macroalgae under chronic and acute disturbance. *Coral Reefs* 24(4):681–692.
87. Eakin CM, et al. (2010) Caribbean corals in crisis: record thermal stress, bleaching, and mortality in 2005. *PLoS One* 5(11):e13969.
88. Wilkinson CR, Souter D (2008) *Status of Caribbean coral reefs after bleaching and hurricanes in 2005* (Global Coral Reef Monitoring Network, and Reef and Rainforest Research Centre, Townsville).
89. Liu G, Strong AE, Skirving W (2003) Remote sensing of sea surface temperatures during 2002 barrier reef coral bleaching. *Eos Trans Am Geophys Union* 84(15):137–141.
90. Manzello DP, et al. (2007) Hurricanes benefit bleached corals. *Proc Natl Acad Sci* 104(29):12035–12039.

91. Van Woesik R, Irikawa A, Loya Y (2004) Coral bleaching: signs of change in southern Japan. *Coral Health and Disease*, eds Rosenberg E, Loya Y (Springer Berlin Heidelberg), pp 119–141.
92. McField MD (1999) Coral response during and after mass bleaching in Belize. *Bull Mar Sci* 64(1):155–172.
93. Strong AE, Barrientos CS, Duda C, Sapper J (1997) Improved satellite techniques for monitoring coral reef bleaching. *Proc 8th Int Coral Reef Symp* 2:1495–1498.
94. CARICOMP (1997) Studies on Caribbean coral bleaching, 1995-96. *Proc 8th Int Coral Reef Symp* 1:673–678.
95. Lang JC, et al. (1992) Spatial and temporal variability during periods of "recovery" after mass bleaching on Western Atlantic coral reefs. *Am Zool* 32(6):696–706.
96. Caley MJ, et al. (1996) Recruitment and the local dynamics of open marine populations. *Annu Rev Ecol Syst* 27(1):477–500.
97. Edmunds PJ (2004) Juvenile coral population dynamics track rising seawater temperature on a Caribbean reef. *Mar Ecol Prog Ser* 269:111–119.
98. De'ath G, Lough JM, Fabricius KE (2009) Declining coral calcification on the Great Barrier Reef. *Science* 323(5910):116–119.
99. Bozec Y-M, Mumby PJ (2015) Synergistic impacts of global warming on the resilience of coral reefs. *Philos Trans R Soc B* 370(1659):20130267.
100. Roff G, Mumby PJ (2012) Global disparity in the resilience of coral reefs. *Trends Ecol Evol* 27(7):404–413.
101. Steneck RS, Arnold SN, Mumby PJ (2014) Experiment mimics fishing on parrotfish: insights on coral reef recovery and alternative attractors. *Mar Ecol Prog Ser* 506:115–127.
102. Steneck RS, Arnold SN, Rasher DB (2013) *Status and trends for Bonaire's reefs in 2013: Causes for optimism*.
103. Walsh WJ (1983) Stability of a coral reef fish community following a catastrophic storm. *Coral Reefs* 2(1):49–63.
104. Woodley JD, et al. (1981) Hurricane Allen's impact on Jamaican coral reefs. *Science* 214:13.
105. Kaufman LS (1983) Effects of Hurricane Allen on reef fish assemblages near Discovery Bay, Jamaica. *Coral Reefs* 2(1):43–47.
106. Gilmour JP, Smith LD, Heyward AJ, Baird AH, Pratchett MS (2013) Recovery of an isolated coral reef system following severe disturbance. *Science* 340(6128):69–71.
107. Alvarez-Filip L, Dulvy NK, Gill JA, Côté IM, Watkinson AR (2009) Flattening of Caribbean coral reefs: region-wide declines in architectural complexity. *Proc R Soc B Biol Sci* 276(1669):3019–3025.
108. Bozec Y-M, Alvarez-Filip L, Mumby PJ (2015) The dynamics of architectural complexity on coral reefs under climate change. *Glob Change Biol* 21(1):223–235.
109. Roff G, Zhao J, Mumby PJ (2015) Decadal-scale rates of reef erosion following El Niño-related mass coral mortality. *Glob Change Biol* 21(12):4415–4424.
110. Bozec Y-M, Yakob L, Bejarano S, Mumby PJ (2013) Reciprocal facilitation and non-linearity maintain habitat engineering on coral reefs. *Oikos* 122(3):428–440.